Journal of Alloys and Compounds 681 (2016) 444–454

Contents lists available at ScienceDirect

Journal of Alloys and Compounds

journal homepage: http://www.elsevier.com/locate/jalcom

Synthesis of new double perovskites $La_{1.98}Mn_{1.11}Mo_{0.89}O_{5.93}$ and $La_{1.92}Mn_{1.29}Mo_{0.71}O_{5.84}$: Characterization of structural and magnetic properties

V. Fuster [a], M.C. Blanco [b], D.G. Franco [c], G. Tirao [d], V.M. Nassif [e], G. Nieva [c], R.E. Carbonio [b, *]

[a] Instituto de Física de Rosario (CONICET-UNR), Bv. 27 de Febrero 210 bis, 2000, Rosario, Argentina
[b] INFIQC (CONICET-UNC), Departamento de Fisicoquímica, Facultad de Ciencias Químicas, Universidad Nacional de Córdoba, Haya de la Torre esq, Medina Allende, Ciudad Universitaria, X5000HUA, Córdoba, Argentina
[c] Centro Atómico Bariloche, Comisión Nacional de Energía Atómica (CNEA) and Instituto Balseiro (UNCuyo), Av. Ezequiel Bustillo 9500, 8400 S. C, de Bariloche, Argentina
[d] IFEG (CONICET), Facultad de Matemáticas, Astronomía y Física, Universidad Nacional de Córdoba, Haya de la Torre esq, Medina Allende, X5000HUA, Córdoba, Argentina
[e] CNRS, Institut NÉEL, 25 Avenue des Martyrs, 38042, Grenoble, France

ARTICLE INFO

Article history:
Received 13 January 2016
Received in revised form
7 April 2016
Accepted 18 April 2016
Available online 26 April 2016

Keywords:
Magnetically ordered materials
Crystal structure
Vacancy formation
Magnetic measurements
Neutron diffraction
Order-disorder effects

ABSTRACT

The synthesis, structural and magnetic characterization of two new perovskites $La_{1.98}Mn_{1.11}Mo_{0.89}O_{5.93}$ and $La_{1.92}Mn_{1.29}Mo_{0.71}O_{5.84}$ are reported. Combined Rietveld refinements of X-ray and neutron powder diffraction data indicate that both samples are monoclinic perovskites with space group $P2_1/n$. The distribution of the transition metals over the octahedral sites is highly ordered: Mn preferentially occupies *2c* sites, while Mo mostly occupies *2d* sites. Mn oxidation states were determined by means of high resolution Kβ Emission Spectroscopy. The susceptibility as a function of temperature measurements and hysteresis loops show complex magnetic behaviour of both perovskites. The refined magnetic cells indicate that $La_{1.98}Mn_{1.11}Mo_{0.89}O_{5.93}$ is ferrimagnetic as a result of the antiferromagnetic coupling of two ferromagnetic sub-lattices associated to *2d* and *2c* sites, while $La_{1.92}Mn_{1.29}Mo_{0.71}O_{5.84}$ is ferromagnetic due to ferromagnetic alignment of the two sub-lattices. The magnetic overall behaviour of the latter perovskite is interpreted in terms of delocalization of magnetic moments arising from ferromagnetic double-exchange interactions between Mn^{2+} and Mn^{3+}.

1. Introduction

Double perovskites are intensively studied since the discovery of the colossal magnetoresistant at room temperature Sr_2FeMoO_6 [1]. The flexibility to accommodate many different cations in the A, B and B′ sites of the general formula $A_2BB'O_6$ gives a large versatility for the synthesis of new compounds with properties that can be tailored adequately. Particularly, the proper combination of B and B′ ions can drive many interesting magnetic properties [2–5]. Moreover, the variation in stoichiometry, particularly the relation between B and B′ can change dramatically the magnetic properties [6,7]. It was shown previously that compounds with the stoichiometry $A_3B_2B'O_9$ (where B is a magnetic ion and B′is a diamagnetic one) have larger T_C values than the corresponding $A_2BB'O_6$ compounds [8]. On the other hand, if B is a magnetic ion and B′ belongs to the second or third transition metals series, because of the large delocalization of the 4d and 5d electrons, half metallic compounds, usually with magnetoresistant properties at room temperature are obtained [9]. The itinerant nature of Mo^{4+} and Mo^{5+} electrons and their distribution among 3d and 4d orbitals was confirmed by Chmaissem et al. [10].

We have studied the Mn^{2+} containing double perovskite $BaLaMnSbO_6$ [5] and found interesting magnetic properties. This compound displays signs of superparamagnetism in the 40–160 K range, which arises from unbalanced antiferromagnetism inside nanoclusters formed by regions which are rich in Mn^{2+}–O^{2-}–Mn^{2+} paths. The possibility of Zener double exchange

* Corresponding author.
E-mail address: carbonio@fcq.unc.edu.ar (R.E. Carbonio).

http://dx.doi.org/10.1016/j.jallcom.2016.04.169
0925-8388/

for the similar compound $SrLaMnSbO_6$ has been reported by Greenblath and co-workers [11].

Recently, ordered Mo double perovskites $Sr_2Mg_{1-x}Mn_xMoO_{6-\delta}$ and $Sr_2MgMoO_{6-\delta}$ have been characterized as promising materials for Solid Oxide Fuel Cells (SOFCs) [12,13]. Mo, a 4d transition metal which can be tetravalent ($4d^2$, t_{2g}^2, S = 1), pentavalent ($4d^1$, t_{2g}^1, S = 1/2) or hexavalent ($4d^0$, t_{2g}^0, S = 0), can be adapted to any other B′ cation by just regulating the synthesis conditions (oxidizing or reducing atmospheres).

Based on these facts, we synthesize two new double perovskites with general compositions $La_{2-z}Mn_{1+x}M_{1-x}O_{6-\delta}$, particularly $La_{1.98}Mn_{1.11}Mo_{0.89}O_{5.93}$ and $La_{1.92}Mn_{1.29}Mo_{0.71}O_{5.84}$. We make their structural characterization using powder X-ray diffraction (PXRD) and powder neutron diffraction (PND), and magnetic characterization using Magnetization (M) vs. Temperature and M vs. Magnetic field (H) measurements. The oxidation states of Mn were determined by high-resolution X-ray emission spectroscopy (XES) [14].

The objective of this work is to try to find new magnetic materials and to see how changes in composition of the two transition metal cations (the magnetic one (Mn^{2+}) and the one that provides the itinerant electrons ($Mo^{4/5+}$)) affect these magnetic properties.

2. Materials and methods

Two $La_{2-z}Mn_{1+x}M_{1-x}O_{6-\delta}$ double perovskites were obtained as well-crystallized powders by the standard ceramic method. Stoichiometric amounts of analytical grade La_2O_3, MnO and MoO_2 (Strem Chemicals) were mixed and ground in agate mortar and pressed into small discs to reduce surface exposure to air. The pellets were placed into an alumina crucible and between two other crucibles with Ti turnings as oxygen getters and heat-treated at 1400 °C for 12 h in Ar atmosphere. The reducing atmosphere was selected in order to stabilize $Mo^{4+/5+}$ oxidation states.

The materials were characterized by PXRD recorded at room temperature (RT) using a PANalytical X'Pert Pro diffractometer in Bragg-Brentano reflection geometry operating at 40 kV and 40 mA, with Cu Kα radiation. The scans were performed from 10 to 110°, in 2θ steps of 0.02°, with 8s collecting time. Powder Neutron Diffraction (PND) patterns were collected at D1B and D2B high-resolution lines at Institute Laue Langevin, Grenoble, France. For $La_{1.98}Mn_{1.11}Mo_{0.89}O_{5.93}$ the measurements were performed using λ = 1.287 Å, from 0.1 to 130°, in steps of 0.1°, both at RT and 2K. For $La_{1.92}Mn_{1.29}Mo_{0.71}O_{5.84}$, the diffractograms were collected using λ = 1.59 Å, from 0.1 to 150°, in steps of 0.05°, at RT and 10 K. The structural analysis was done by Rietveld refinement [15] using the Fullprof software [16]. Peak shape was refined with a pseudo-Voigt profile function.

Manganese oxidation state was determined by High-resolution Kβ Emission Spectroscopy [17]. Synthetic standards with known oxidation states were used for comparison purposes with the studied samples. The spectral parameter IAD [18] (integral of the absolute value of the difference between two spectra) was selected for determining the Mn oxidation state, since it uses the whole spectrum information and only requires a simple spectrum pre-analysis: area normalization and $K\beta_{1,3}$ line alignment. It is well known that this parameter is very suitable for oxidation state quantification even considering direct calculations and minor experimental data treatment [19].

Magnetic characterization was performed in a Quantum Design Superconducting Quantum Interference Device magnetometer (SQUID). The magnetic susceptibility data were collected from 5 to 300 K, with an applied field of 0.1 T, after cooling in the absence of a magnetic field (ZFC) and after cooling under an applied magnetic field (FC). The isothermal magnetization curves were collected at 5 K with magnetic fields up to 5 T.

3. Results

3.1. Structural characterization

The formation of both the compounds of interest, $La_{1.98}Mn_{1.11}Mo_{0.89}O_{5.93}$ and $La_{1.92}Mn_{1.29}Mo_{0.71}O_{5.84}$, as majority phases is shown in Figs. 1a and 2a through the corresponding PXRD patterns at RT. $La_{1.98}Mn_{1.11}Mo_{0.89}O_{5.93}$ was accompanied by 4 wt % of La_3MoO_7 (space group *Cmcm* Nº 63). $La_{1.92}Mn_{1.29}Mo_{0.71}O_{5.84}$ contained 4 wt % of $La(OH)_3$, with hexagonal structure (space group P $6_3/m$ Nº 176). From the Rietveld refinement of the RT PND patterns in the monoclinic space group $P2_1/n$, the lattice parameters and the final compositions were obtained. Bazuev et al. [20,21] reported the synthesis of a rhombohedral $LaMn_{2/3}Mo_{1/3}O_3$ perovskite. However, chemically related perovskites such as Sr_2MnMoO_6, Sr_2MnWO_6 and Ca_2MnWO_6 [22,23] have been described as monoclinic with the same space group. Minority phases have also been reported [23].

Phase contents were obtained from conventional multiphase Rietveld refinements of PXRD patterns.

The Goldschmidt tolerance factors *t* were calculated, according to $t = (r_{La} + r_O)/\sqrt{2}[(r_{Mn} + r_{Mo})/2 + r_O]$, before the synthesis for both the ideal stoichiometry La_2MnMoO_6 and $La_2Mn_{4/3}Mo_{2/3}O_6$ perovskites. The r_{La}, r_{Mn}, r_{Mo}, and r_O are the room temperature ionic radii reported by Shannon [24] for the La^{3+} cation (in twelvefold coordination), the Mn^{2+}, $Mo^{4+}$and Mo^{5+} cationic radii (in sixfold coordination), and the oxide anion radius (in twofold coordination). The obtained values were 0.91 for both compositions. When this factor is below unity, the perovskite structure might be of lower symmetry than cubic. Also, this value suggests possible large distortions caused by the cooperative rotation of the BO_6 and $B'O_6$ octahedral networks, as will be discussed later.

Parameters obtained from the Rietveld refinements are summarized in Tables 1–3. The reported final compositions result from refining La, Mn, Mo and O occupancies with PND data. It is important to note that the scattering lengths of Mo and Mn are 6.715 and −3.73 fm, the meaning of these scattering lengths are explained by Sears, V. F. [25]. These scattering lengths are different enough to refine occupancies which are correlated, with a high confidence. In Table 1 the corresponding lattice parameters and occupancies are presented. In Table 2 the Wyckoff sites, the atomic positions and the isotropic temperature factors (B_{iso}) are informed. Selected bond distances and bond angles are shown in Table 3.

Both compounds are monoclinic double perovskites. The unit cell monoclinic distortion is very small, with β-angles very close to 90° (see Table 1). Besides, the octahedral networks exhibit relatively high tilt angles, 15° average (see Table 3 and Fig. 3). The tilt system for this space group is $a^-b^-c^+$, according to Glazer notation [26]. The octahedral tilt angles (δ) were calculated from $(Mn/Mo)_{2d}$–O–$(Mn/Mo)_{2c}$ bond angles (θ), as (180 − θ)/2. The occupancies below unity of La^{3+} and O^{2-} indicate that there are vacancies in A and O sites within the structure, and define the final composition for both double perovskites.

Stoichiometric amounts of pure oxides were mixed to synthesize the ideal La_2MnMoO_6 compound. However, the content of Mn ions is higher than the content of Mo ions in the $La_{1.98}Mn_{1.11}Mo_{0.89}O_{5.93}$ perovskite. Consistently, the excess of Mo is still present in the minor phase La_3MoO_7, as illustrated in Fig. 4a. Huang et al. [12,13] mentioned that when there are oxygen vacancies the double perovskite structure remains unchanged if the two octahedral-site cations are stable in less than six-fold oxygen coordination. It is possible that the structure of the ordered octahedral network of $La_{1.98}Mn_{1.11}Mo_{0.89}O_{5.93}$ perovskite is stabilized with a higher proportion of the more stable Mn^{2+} ion, in comparison to Mo^{4+}/Mo^{5+}

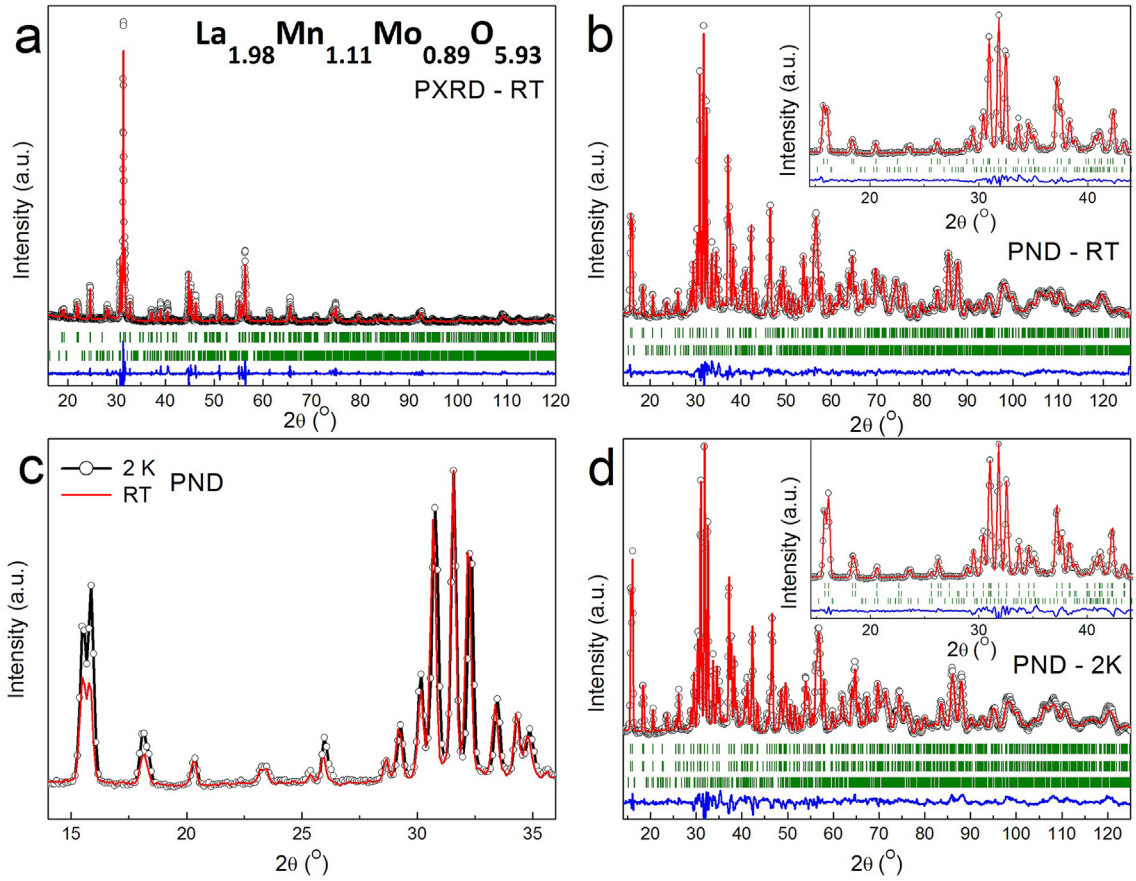

Fig. 1. Diffraction patterns of $La_{1.98}Mn_{1.11}Mo_{0.89}O_{5.93}$: **a)** PXRD pattern at RT, **b)** PND pattern at RT, **c)** Superimposed both RT (full line) and 2K (circles) PND patterns in the low angle region, showing the intensity increase of some peaks due to long range magnetic coupling at 2 K, and d) PND pattern at 2 K. In **a)**, **b)** and **d)** observed (circles), calculated (full line), difference (bottom line) between observed and calculated patterns and Bragg positions (vertical bars); **Upper bars**: $La_{1.98}Mn_{1.11}Mo_{0.89}O_{5.93}$, **Lower bars**: La_3MoO_7, Middle bars (only in d): magnetic phase. **Insets**: Detail of the Rietveld refinements in the low angle regions.

ions, in those sites.

$La_{1.92}Mn_{1.29}Mo_{0.71}O_{5.84}$, was initially prepared as $La_2Mn_{1.33}Mo_{0.67}O_6$ double perovskite. From the refined composition it can be seen that the ratio between Mn and Mo ions is near to the planned one. But this material has more La and O vacancies than $La_{1.98}Mn_{1.11}Mo_{0.89}O_{5.93}$. An interesting feature is the lower stability for this perovskite, which could be tested by a new PXRD data measured two years after the synthesis. Fig. 4b shows the segregation of more minor phase $La(OH)_3$ for $La_{1.92}Mn_{1.29}Mo_{0.71}O_{5.84}$, while Fig. 4a illustrate the higher stability of $La_{1.98}Mn_{1.11}Mo_{0.89}O_{5.93}$ for the same time period.

The different stability of these perovskites could be related to the difference in the relative Mn/Mo ion content. The Mn/Mo ratio of the less stable $La_{1.92}Mn_{1.29}Mo_{0.71}O_{5.84}$ perovskite is 1.82, while it is 1.25 for the more stable $La_{1.98}Mn_{1.11}Mo_{0.89}O_{5.93}$.

In several works on highly ordered A_2MMoO_6 double perovskites with oxygen vacancies [12,13,27], Mo^{4+} and Mo^{5+} cations in octahedral sites have been accompanied by M(II) ions as octahedral partners. Similar $A_2(B)(B_{1/3}B'_{2/3})O_6$ double perovskites where B′ is Mo^{4+} or Mo^{5+} have not been described.

A systematic study varying the Mn/Mo ratio, *i.e.* exploring the stability of other members of the $La_2Mn_{1+x}Mo_{x-1}O_6$ family, would be pertinent to elucidate this point.

A closer look at Table 3 shows that (Mn/Mo–O) bond distances associated to *2c* octahedral sites are longer than the *2d* site corresponding lengths, for the two members of this family. At RT and LT the same trend is observed. This is a consequence of the higher Mn content in *2c* octahedral cavities. We corroborated this comparing the experimental and theoretical (B/B′)-O bond lengths according to the ionic radii [24]. The average bond distances for 2*c* sites are in good agreement with the calculated ones, considering that each site contains only Mn^{2+} ions (2.18 Å). Also, the average bond distances for 2*d* sites are compatible with the expected ones, assuming that every site is primarily occupied by Mo^{5+} ions (1.97 Å).

A measurement of the regularity of octahedra is the distortion index (Δd). This factor compares the individual (B/B′)–O bond lengths (d_i) to the average (B/B′)–O length (d_{ave}) reported in Table 3, and is calculated according to Eq. (1) at RT and LT. The Δd values at RT and LT are summarized in Table 4.

$$\Delta d = \frac{1}{6}\sum_{i=1}^{6}\left(\frac{d_i - d_{ave}}{d_{ave}}\right)^2 \quad (1)$$

Δd would be zero if the octahedra were completely undistorted, but for lower symmetry space groups, small non-zero Δd values are expected. Octahedra with significant distortions of the bond lengths have Δd values greater than 10^{-3} [28]. All calculated Δd values lie within the range previously determined for other perovskites [28,29] and indicate that every octahedron in both perovskites is not ideally symmetric. The deviation from symmetry of the octahedra in both perovskite increases as temperature decreases. In $La_{1.98}Mn_{1.11}Mo_{0.89}O_{5.93}$ low Δd indices were obtained for *2c* sites, preferentially occupied by Mn cations (see Table 1), so this points to spherical Mn^{2+} $3d^5$ ($t_{2g}^3e_g^2$). In $La_{1.92}Mn_{1.29}Mo_{0.71}O_{5.84}$ Δd

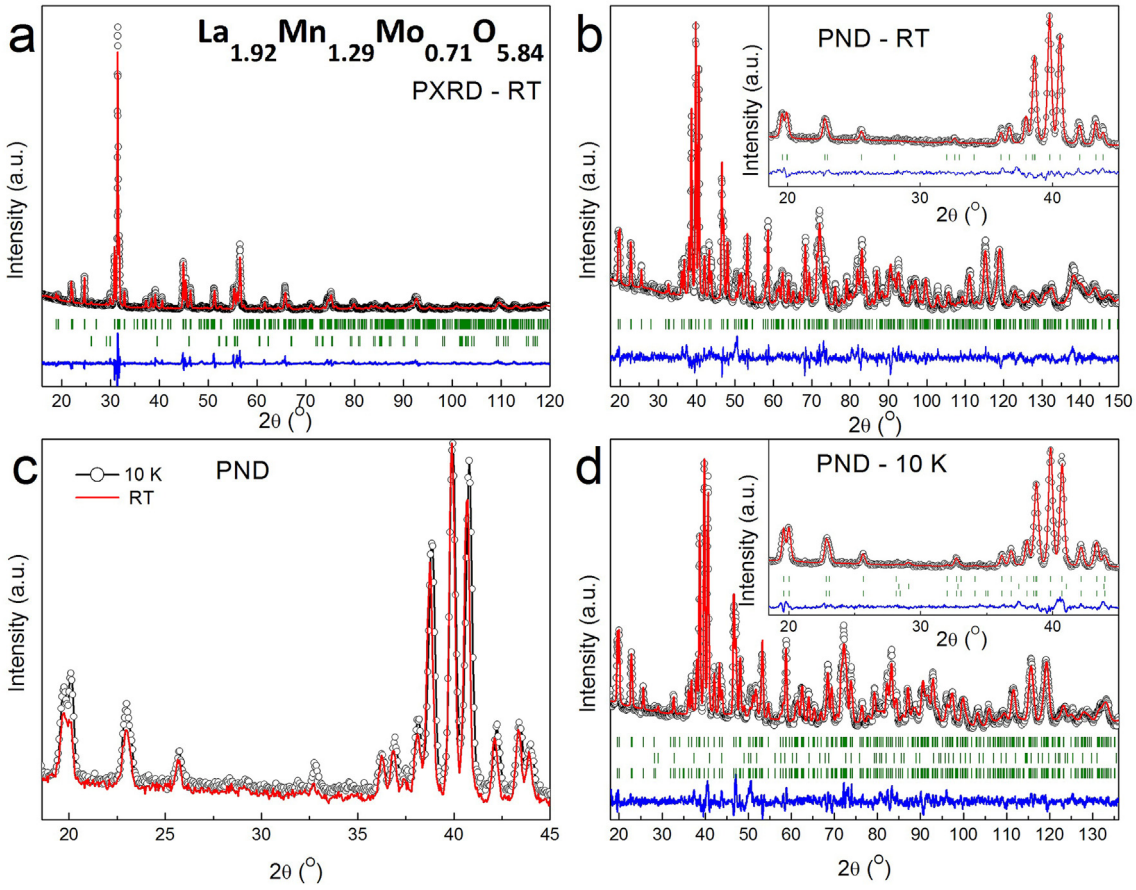

Fig. 2. Diffraction patterns of $\mathbf{La_{1.92}Mn_{1.29}Mo_{0.71}O_{5.84}}$: **a)** PXRD pattern at RT, **b)** PND pattern at RT, **c)** Superimposed both RT (full line) and 10 K (circles) PND patterns in the low angle region, showing the intensity increase of some peaks due to long range magnetic coupling at 10 K, and **d)** PND pattern at 10 K. In **a)**, **b)** and **d)** observed (circles), calculated (full line), difference (bottom line) between observed and calculated patterns and Bragg positions (vertical bars); Upper bars: $La_{1.92}Mn_{1.29}Mo_{0.71}O_{5.84}$, **Lower bars**: $La(OH)_3$, Lower bars (only in d): magnetic phase. **Insets**: Detail of the Rietveld refinements in the low angle regions.

Table 1
Lattice parameters (*a, b, c, β*), cell volume (*V*), occupancy factors (*Occ.*) and reliability factors (R_{Bragg}, R_{wp}) of $\mathbf{La_{1.98}Mn_{1.11}Mo_{0.89}O_{5.93}}$ and $\mathbf{La_{1.92}Mn_{1.29}Mo_{0.71}O_{5.84}}$ double perovskites, determined from combined Rietveld refinement of PXRD and PND data at RT and 2 K.

	$La_{1.98}Mn_{1.11}Mo_{0.89}O_{5.93}$		$La_{1.92}Mn_{1.29}Mo_{0.71}O_{5.84}$	
	300 K	2 K	300 K	10 K
a (Å)	5.6301(1)	5.6167(2)	5.6099(4)	5.5923(4)
b (Å)	5.8021(1)	5.8081(2)	5.7700(3)	5.7686(4)
c (Å)	8.0020(2)	7.9731(3)	7.9711(5)	7.9514(5)
β (°)	90.009(1)	90.031(1)	89.98(1)	90.01(2)
V (Å^3)	261.4(1)	260.10(2)	258.02(3)	256.51(3)
Occ. La$_{4e}$	0.991(1)		0.961(1)	
Occ. (Mn/Mo)$_{2d}$	0.120(1)/0.880(1)		0.300(1)/0.700(1)	
Occ. (Mn/Mo)$_{2c}$	0.988(1)/0.012(1)		1.000/0.000	
Occ. O1$_{4e}$	1		1	
Occ. O2$_{4e}$	1		1	
Occ. O3$_{4e}$	0.964(1)		0.922(1)	
$\mathbf{R_{Bragg}}$	4.1	7.1	8.3	9.1
$\mathbf{R_{wp}}$	7.73	10.8	18.0	19.3
Minor phase	4% La_3MoO_7		4% $La(OH)_3$	

increases for the same site, implying that a certain amount of Mn^{3+} $3d^4$ ($t_{2g}^3e_g^1$) might be present.

The 2*d* sites, which are occupied mainly by Mo ions, show a small distortion for $La_{1.98}Mn_{1.11}Mo_{0.89}O_{5.93}$, and a higher one for $La_{1.92}Mn_{1.29}Mo_{0.71}O_{5.84}$. The 2*d* sites occupancies, in Table 1, show a higher content of Mn ions for $La_{1.92}Mn_{1.29}Mo_{0.71}O_{5.84}$ as compared with $La_{1.98}Mn_{1.11}Mo_{0.89}O_{5.93}$. Δ*d* at RT and LT for $La_{1.92}Mn_{1.29}Mo_{0.71}O_{5.84}$ are one order of magnitude higher than the respective Δ*d* values for $La_{1.98}Mn_{1.11}Mo_{0.89}O_{5.93}$, see Table 4. By detailed examination of this site occupancy in Table 1 a minor Mo content is found, but the Mn amount is still significant. The noticeable structural distortion of $La_{1.92}Mn_{1.29}Mo_{0.71}O_{5.84}$ might be another reason why this perovskite gradually evolves into a mixture of its constituent oxides.

At this point it became necessary to measure Mn cation oxidation states, to determine the overall chemical composition of these perovskites.

3.2. Spectroscopic characterization

From spectroscopic characterization the average oxidation states for Mn ions inside the octahedral sites are obtained and are listed in Fig. 5b. Previous works have found the same Mn oxidation states in $BaLaMnMoO_6$ [30], Sr_2MnMoO_6 [22] and A_2MnMoO_6 (A = Ba, Sr) [31]. From the joint study of these results and the compositions obtained from PND it was possible to calculate the formulas: $La^{3+}_{1.98}Mn^{2+}_{1.11}Mo^{4+}_{0.75}Mo^{5+}_{0.14}O^{2-}_{5.93}$ and $La^{3+}_{1.92}Mn^{2+}_{1.16}Mn^{3+}_{0.13}Mo^{4+}_{0.34}Mo^{5+}_{0.37}O^{2-}_{5.84}$. It is clear that the first perovskite has lower valence transition metal cations and has no Mn^{3+} and the second one has higher valence transition metal cations and has some Mn^{3+}. This is important since we will assign the particular magnetic properties to the absence or presence of Mn^{3+}. Also the presence of Mo^{4+} and Mo^{5+} cations will be the

Table 2
Refined atomic positions (*x*, *y*, *z*) and thermal isotropic factors (B_{iso}) of **$La_{1.98}Mn_{1.11}Mo_{0.89}O_{5.93}$** and **$La_{1.92}Mn_{1.29}Mo_{0.71}O_{5.84}$**, from PND data at RT and Low Temperature (LT).

	Ion	Site	T (K)	x	y	z	B_{iso}
$La_{1.98}Mn_{1.11}Mo_{0.89}O_{5.93}$	**La**	4e	300	0.5128(3)	0.5519(2)	0.2488(2)	0.78(2)
			2	0.5160(4)	0.5528(3)	0.2519(3)	0.80(3)
	Mn/Mo	2d	300	0.5	0	0	0.57(7)
			2				0.89(7)
	Mn/Mo	2c	300	0	0.5	0	0.49(4)
			2				0.97(4)
	O1	4e	300	0.1884(4)	0.2109(4)	−0.0509(3)	0.68(5)
			2	0.1791(4)	0.2139(4)	−0.0538(3)	1.03(5)
	O2	4e	300	0.2912(4)	0.6938(4)	−0.0474(4)	0.87(4)
			2	0.2876(4)	0.6903(4)	−0.0507(3)	0.56(5)
	O3	4e	300	0.4049(3)	−0.0283(2)	0.2590(3)	0.74(3)
			2	0.4038(4)	−0.0297(3)	0.2641(4)	0.81(5)
$La_{1.92}Mn_{1.29}Mo_{0.71}O_{5.84}$	**La**	4e	300	0.5119(6)	0.5510(4)	0.2546(7)	0.66(7)
			10	0.5127(6)	0.5530(4)	0.2520(7)	0.79(5)
	Mn/Mo	2d	300	0.5	0	0	1.09(5)
			10				1.22(4)
	Mn/Mo	2c	300	0	0.5	0	1.21(5)
			10				1.20(4)
	O1	4e	300	0.2078(2)	0.2036(1)	−0.0528(2)	1.70(5)
			10	0.1924(2)	0.1924(2)	−0.0468(2)	1.71(4)
	O2	4e	300	0.3021(2)	0.6991(2)	−0.0416(2)	0.93(4)
			10	0.3044(2)	0.7061(2)	−0.0472(2)	0.99(4)
	O3	4e	300	0.4121(2)	−0.0228(1)	0.2436(2)	0.84(4)
			10	0.4080(2)	−0.0261(1)	0.2412(2)	0.83(4)

Table 3
Refined $(Mn/Mo)_{2d}$–O and $(Mn/Mo)_{2c}$–O bond distances, B–O–B′ angles and tilt angles (δ) at RT and LT, for both double perovskites. Tilt angles were obtained according to δ = (180° - (θ))/2.

	T (K)		O1	O2	O3	Average
$La_{1.98}Mn_{1.11}Mo_{0.89}O_{5.93}$	300	$(Mn/Mo)_{2d}$–O (Å)	2.025(1)	2.024(1)	2.009(1)	2.019
	2		1.990(1)	1.999(1)	1.964(1)	1.984
	300	$(Mn/Mo)_{2c}$–O (Å)	2.176(1)	2.164(1)	2.147(1)	2.162
	2		2.230(1)	2.196(1)	2.181(1)	2.202
	300	B–O–B′ (°)	148.4(1)	149.6(1)	148.6(1)	148.9
	2		146.4(1)	148.7(1)	148.1(1)	147.7
	300	δ (°)	15.8	15.2	15.7	15.6
	2		16.8	15.7	16.0	16.2
$La_{1.92}Mn_{1.29}Mo_{0.71}O_{5.84}$	300	$(Mn/Mo)_{2d}$–O (Å)	2.060(1)	2.087(1)	2.008(2)	2.052(1)
	10		1.990(2)	2.052(1)	1.991(3)	2.011(1)
	300	Mn_{2c}–O (Å)	2.112(1)	2.074(1)	2.107(2)	2.098(1)
	10		2.167(1)	2.110(2)	2.127(3)	2.135(1)
	300	B–O–B′ (°)	149.3(1)	150.5(1)	151.3(1)	150.4(1)
	10		150.2(1)	149.7(1)	149.8(1)	149.9(1)
	300	δ (°)	15.4	14.8	14.4	14.8
	10		14.9	15.2	15.1	15.1

reason for the presence of itinerant electrons.

3.3. Magnetic characterization

The Magnetization (M) as a function of temperature (T) of both double perovskites was measured with a 0.1 T applied field (H) under ZFC and FC conditions, and the corresponding Susceptibility (χ) curves are depicted in Fig. 6, left axis. The compounds show spontaneous magnetization below 150 K for $La_{1.98}Mn_{1.11}Mo_{0.89}O_{5.93}$, and below 100 K in the case of $La_{1.92}Mn_{1.29}Mo_{0.71}O_{5.84}$. The transition temperature T_C was determined as the minimum in $\delta M/\delta T$ vs. T. T_C of $La_{1.98}Mn_{1.11}Mo_{0.89}O_{5.93}$ is around 50 K higher than the T_C of $La_{1.92}Mn_{1.29}Mo_{0.71}O_{5.84}$ (see Table 5). Magnetic irreversibility between ZFC and FC curves at temperatures lower than T_C is observed in both perovskites. The curves of $La_{1.98}Mn_{1.11}Mo_{0.89}O_{5.93}$ diverge irreversibly below 126 K, and those of $La_{1.92}Mn_{1.29}Mo_{0.71}O_{5.84}$ diverge below 78 K. From the shape of $La_{1.92}Mn_{1.29}Mo_{0.71}O_{5.84}$ curve this perovskite shows a classic ferromagnetic-like behaviour at LT. Strikingly, this is not the case for $La_{1.98}Mn_{1.11}Mo_{0.89}O_{5.93}$ whose magnetization thermal evolution is quite complex. Further magnetic study of this material is required, analyzing the M vs T behaviour under different applied fields.

The inverse of susceptibility (χ^{-1}) vs. T for both perovskites was fitted according to the Curie-Weiss law $H/M = (T - \theta_{Weiss})/C$ in the high temperature region, between 250 and 300 K (right axis, Fig. 6). The Weiss temperatures (θ_{Weiss}) and the experimental effective magnetic moments (μ_{exp}), calculated from the Curie constant C, are shown in Table 5. We have included the global theoretical effective magnetic moments (μ_{theo}) for the sake of comparison, obtained from $\mu^2_{theo} = a\,\mu^2_t(Mn^{2+}) + b\,\mu^2_t(Mn^{3+}) + c\,\mu^2_t(Mo^{4+}) + d\,\mu^2_t(Mo^{5+})$, where a, b, c and d are stoichiometric coefficients of the corresponding magnetic cations, and $\mu_t = g\,(J\,(J+1))^{1/2}$. Only spin contribution to the theoretical magnetic moments are expected for *3d* transition metals (Mn), whereas for *4d* transition metal (Mo) both spin only (Mo_S) and spin plus orbital contribution (Mo_J) possibilities were considered for the calculation of μ_{theo} in Table 5. We see that μ_{exp} are lower than μ_{theo}. The positive θ_{Weiss} values suggest predominant ferromagnetic interactions within both structures.

The maximum in the ZFC χ curves, and the plateau in the FC curves could suggest a spin freezing below $T_F \approx 55$ and 54 K

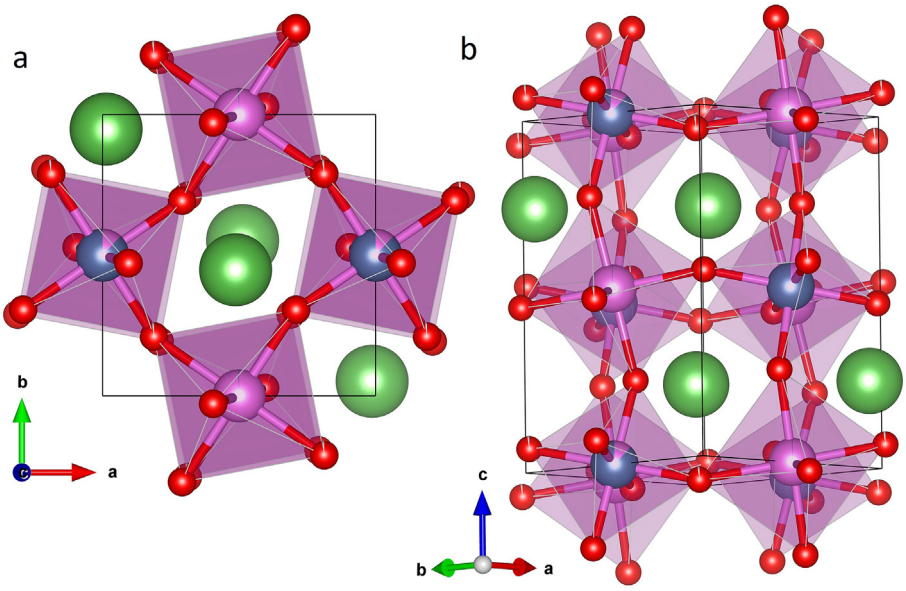

Fig. 3. Polyhedral views of the monoclinic structure of $\mathbf{La_{1.98}Mn_{1.11}Mo_{0.89}O_{5.93}}$ double perovskite at 300 K: a) [001] view of in-phase, and b) [110] view of anti-phase rotation of the $(Mn/Mo)_{2d}O_6$ and $(Mn/Mo)_{2c}O_6$ octahedral networks corresponding to the tilt system $a^-b^-c^+$. La (big spheres), Mn and Mo (spheres inside the octahedra), O (small spheres).

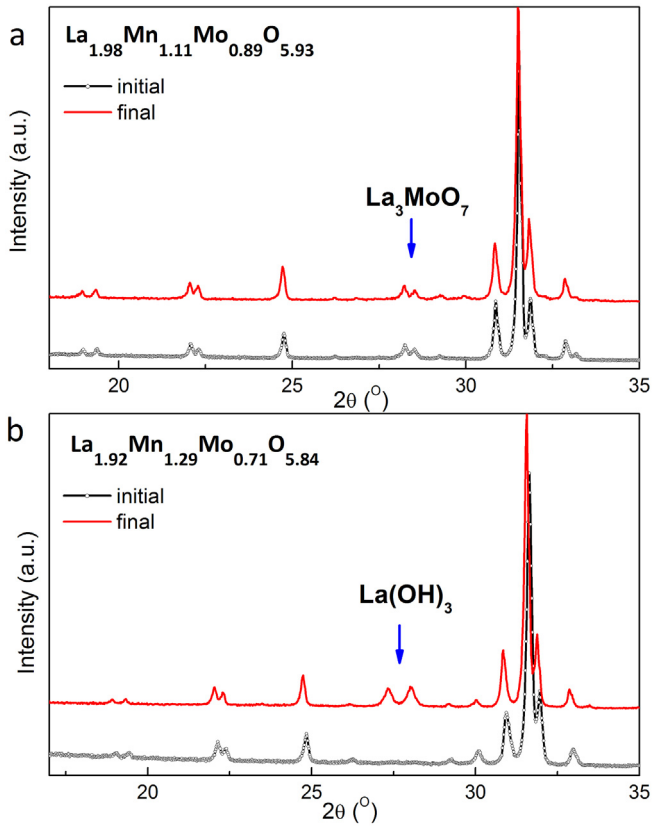

Fig. 4. Comparison of PXRD patterns taken immediately after synthesis and after 2 years **a)** $\mathbf{La_{1.98}Mn_{1.11}Mo_{0.89}O_{5.93}}$ and **b)** $\mathbf{La_{1.92}Mn_{1.29}Mo_{0.71}O_{5.84}}$ double perovskites at RT (300 K). Initial (line and circles) and final (solid line) patterns with a two years difference between them.

respectively, for the two studied perovskites [32,33].

Hysteresis loops M vs. H under ZFC conditions measured for both perovskites at 5 K are represented in Fig. 7. Pronounced

Table 4
Average octahedral distortions Δd calculated from Eq. (1)

	T (K)		$\Delta d \times 10^{-5}$
$\mathbf{La_{1.98}Mn_{1.11}Mo_{0.89}O_{5.93}}$	300	$(Mn/Mo)_{2d}$–O	1.3
	2		5.6
	300	$(Mn/Mo)_{2c}$–O	3.0
	2		8.7
$\mathbf{La_{1.92}Mn_{1.29}Mo_{0.71}O_{5.84}}$	300	$(Mn/Mo)_{2d}$–O	26
	10		21
	300	Mn_{2c}–O	6.5
	10		12

hysteresis is observed in the whole range of applied magnetic fields indicating overall ferro or ferrimagnetic behaviour.

The saturation magnetization (M_S) and remanent magnetization (M_R) are included in Fig. 7a. M_S equals 2.5 μ_B/mol, higher than previously reported values in similar perovskite systems, though with a B′ cation different from Mo [2,3,7]. Net magnetic moments around ~2.8 μ_B/f.u. are consistent with ferromagnetic double perovskite Sr_2FeMoO_6 [10,34,35]. The coercive field (H_C) was determined as an average between the positive and negative value at M = 0.

When the M vs. H curve of $La_{1.92}Mn_{1.29}Mo_{0.71}O_{5.84}$ is examined, a step like or double hysteresis behaviour is observed at low fields. The complex hysteresis loop is composed of an irreversible part in almost all the measured range, superimposed to an easily magnetisable component at low fields. A combination of interacting softer and harder magnetic phases present in the material may be responsible for such behaviour. M_S and M_R of this perovskite are higher in comparison with $La_{1.98}Mn_{1.11}Mo_{0.89}O_{5.93}$ results and H_C was not determined, because of the step like behaviour.

In both perovskites the initial curve (Fig. 7, b and d) lays outside the hysteresis loop at 5 K. Such behaviour can be an indication for frustration, cationic disorder, spin glass behaviour [32] and irreversible domain-wall motion [6,36]. Cationic disorder is actually present in both perovskites, and the extension of such disorder is higher for the second material. It is initially difficult to ensure frustration because of the ferromagnetic-like characteristics of the perovskites.

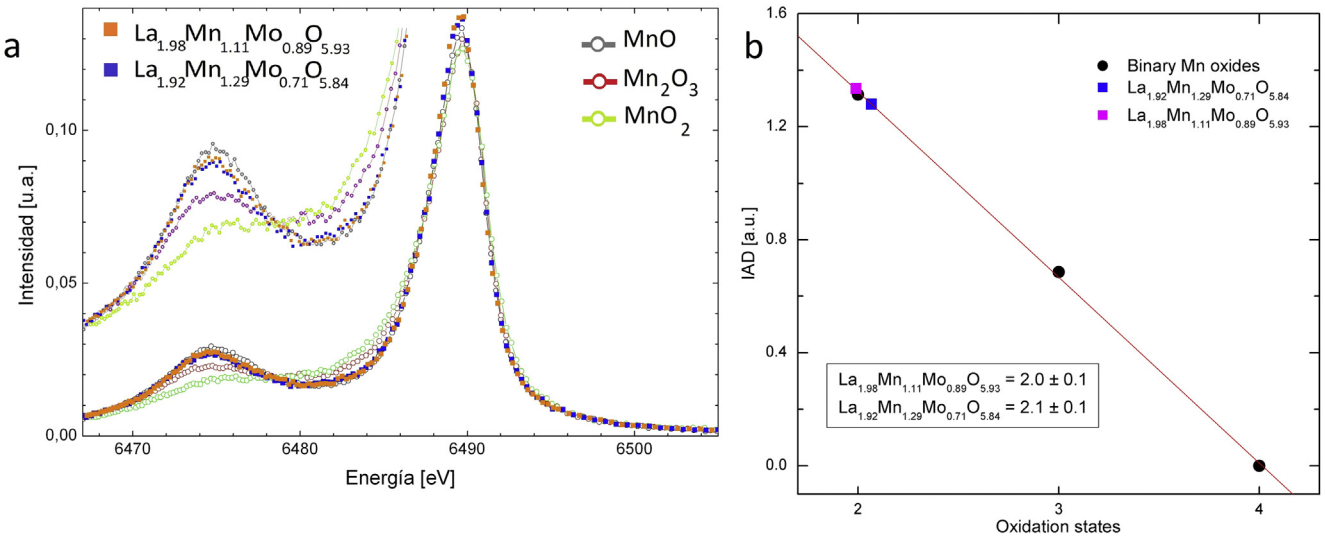

Fig. 5. a) High-resolution Mn-Kβ emission spectrum in the Kβ main region (Kβ′ and $K\beta_{1,3}$) for known binary Mn oxides and double perovskites **$La_{1.98}Mn_{1.11}Mo_{0.89}O_{5.93}$** and **$La_{1.92}Mn_{1.29}Mo_{0.71}O_{5.84}$** and **b)** IAD calculated value as a function of oxidation states of Mn oxides and compounds. The oxidation state of Mn in studied double perovskites is obtained from the linear regression (red line) of binary oxides. The IAD errors are less than the dots dimension. (For interpretation of the references to colour in this figure legend, the reader is referred to the web version of this article.)

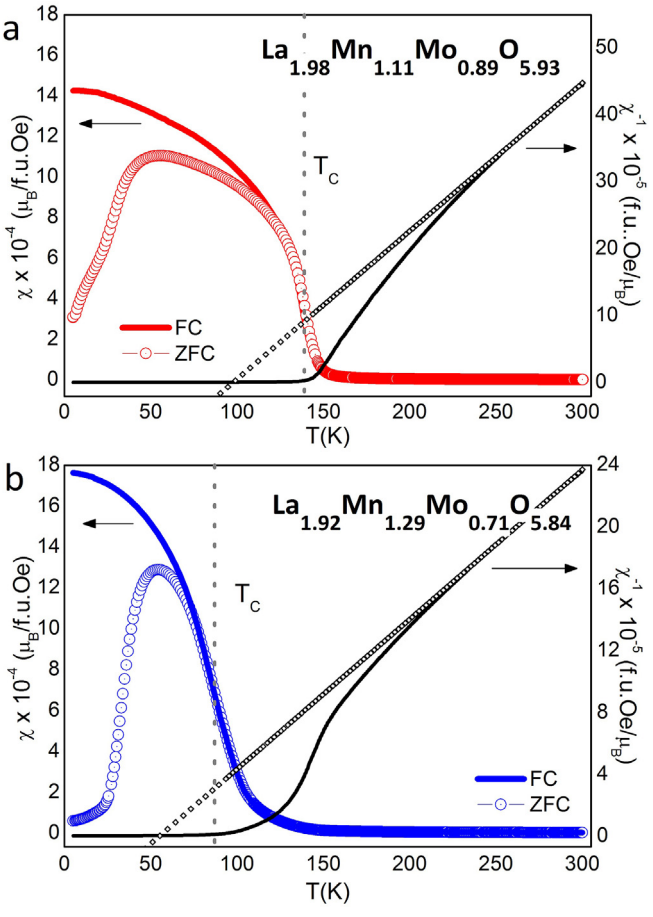

Fig. 6. χ (left axis) and χ^{-1} (right axis) vs. T for **a)** **$La_{1.98}Mn_{1.11}Mo_{0.89}O_{5.93}$** and **b)** **$La_{1.92}Mn_{1.29}Mo_{0.71}O_{5.84}$**, measured at 0.1 T under FC (solid line) and ZFC (empty circles) conditions. Straight lines represent the linear fits of the Curie-Weiss law in the paramagnetic region (250–300 K). Vertical dotted lines stand for the Curie temperatures (T_c), taken as the minima of the $\delta M/\delta T$ vs T curves.

The possibility of long range magnetic order can be analysed in the LT PND patterns and compared with magnetic behaviour previously discussed. In Figs. 1c and 2c it is shown the low angle region for both RT and LT PND data. When superimposed, the RT and LT data show differences in the ratio intensities for some diffraction peaks, but no new reflections. This suggests the possibility of some long range magnetic arrangement of ferromagnetic nature. The Rietveld refinements of LT PND data were done including a magnetic cell with the crystalline cell (see Figs. 1d and 2d). In the insets in Figs. 1d and 2d the Rietveld refinements at low angle region are shown. The magnetic cells obtained from the refinements are depicted in Fig. 8, where the arrows correspond to the Mn/Mo cation magnetic moment vectors.

According to the graphical representation of the magnetic cells, the *2c* magnetic moments are more intense than those corresponding to *2d* sites. Also, clearly different macroscopic magnetic behaviour is found for each perovskite.

When $La_{1.98}Mn_{1.11}Mo_{0.89}O_{5.93}$ reaches long range magnetic order, the ferromagnetic arrangement of ions on *2c* sites is collinearly and antiferromagnetically coupled to another ferromagnetic arrangement of ions on *2d* site. The resultant magnetic cell at 2 K is a ferrimagnetic one with a propagation vector $k = 0$ (Fig. 8a), and a total ferrimagnetic moment of around 3.9 μ_B. When individually analysed the magnetic moment measured in *2c* site represent the 83% of total refined magnetic moment and the one in the *2d* site 17%.

Regarding $La_{1.92}Mn_{1.29}Mo_{0.71}O_{5.84}$ perovskite, the two sublattices which are associated to *2c* and *2d* sites are now coupled ferromagnetically (see Fig. 8b). This perovskite has a ferromagnetic cell with $k = 0$ and a total magnetic moment of 3.6 μ_B, which is in agreement with M_S from M vs. H data. Now, the *2c* and *2d* sites represent 78% and 22% of the total magnetic moment respectively.

It is possible to calculate the theoretical magnetic moment per site according to the expression: $\mu_B^{site} = a\mu_{Mn2+} + b\mu_{Mn3+} + c\mu_{Mo4+} + d\mu_{Mo5+}$, where *a*, *b*, *c* and *d* are the stoichiometric coefficients for Mn^{2+}, Mn^{3+}, Mo^{4+} and Mo^{5+} content, respectively. The calculated values for both perovskites are displayed in Table 6. When the refined values obtained from magnetic cells are compared with the theoretical ones, they are

Table 5
Ferromagnetic transition temperature (T_C) and magnetic parameters obtained from linear Curie–Weiss fits: Weiss temperature (θ_{Weiss}), paramagnetic effective moment (μ_{eff}), and theoretical magnetic moment (μ_{teo}).

	$La_{1.98}Mn_{1.11}Mo_{0.89}O_{5.93}$		$La_{1.92}Mn_{1.29}Mo_{0.71}O_{5.84}$	
	ZFC	FC	ZFC	FC
T_C (K)	140	138	89	85
θ_{Weiss} (K)	115	112	64	63
μ_{exp} (μ_B)	3.05	3.09	3.85	3.84
μ_{theo} (μ_B)	Mn^{2+}–Mo^{4+}–Mo^{5+}: 4.75 (Mo_S)–4.54 (Mo_L)		Mn^{2+}–Mn^{3+}–Mo^{4+}–Mo^{5+}: 4.88 (Mo_S)–4.77 (Mo_L)	

lower (Table 6). Even more, from the expressions: $\mu_{total} = |\mu^{2c}_{theo} \pm \mu^{2d}_{theo}|$ it can be estimated the ferro ($\mu^{Ferro}{}_{theo}$) or ferri ($\mu^{Ferri}{}_{theo}$) theoretical total magnetic moment. The final $\mu^{refined}$ from magnetic cells are in between both ferro and ferri cases. Cationic disorder, spin glass behaviour and frustration could be indicated as responsible for these results.

4. Discussion

Two new $La_{2-z}Mn_{x+1}Mo_{1-x}O_{6-\delta}$ double perovskites have been synthesized as black well crystallized powders under identical experimental conditions. Their crystal structures were characterized as monoclinic with $P2_1/n$ space group, though β angles are ~90° so they can be described as pseudo-orthorhombic. On one hand, manganese preferentially occupied *2c* sites, while *2d* content was mainly Mo, and on the other hand, La and O vacancies were found by refining NPD data.

Manganese oxidation states have been determined by XES, and allowed us to determine the Mn cations present in each case, and therefore the final chemical compositions are: $La^{3+}{}_{1.98}Mn^{2+}{}_{1.11}Mo^{4+}{}_{0.75}Mo^{5+}{}_{0.14}O^{2-}{}_{5.93}$ and $La^{3+}{}_{1.92}Mn^{2+}{}_{1.16}Mn^{3+}{}_{0.13}Mo^{4+}{}_{0.34}Mo^{5+}{}_{0.37}O^{2-}{}_{5.84}$.

Their magnetic behaviour differ in many aspects: 1) the $La_{1.98}Mn_{1.11}Mo_{0.89}O_{5.93}$ T_C and θ_{Weiss} temperatures are ~50 K higher than the ones for $La_{1.92}Mn_{1.29}Mo_{0.71}O_{5.84}$; 2) the effective magnetic moments (μ_{eff}) and saturation magnetization (M_S) of $La_{1.98}Mn_{1.11}Mo_{0.89}O_{5.93}$ are below the μ_{eff} and M_S of $La_{1.92}Mn_{1.29}Mo_{0.71}O_{5.84}$; 3) $La_{1.98}Mn_{1.11}Mo_{0.89}O_{5.93}$ magnetic complex behaviour stands when analyzing the magnetization thermal evolution, while $La_{1.92}Mn_{1.29}Mo_{0.71}O_{5.84}$ shows a classical ferromagnetic behaviour; 4) both compounds denote marked irreversibility between ZFC and FC branches during cooling, but in the case of $La_{1.98}Mn_{1.11}Mo_{0.89}O_{5.93}$ this occurs at ~50 K higher temperature with respect to $La_{1.92}Mn_{1.29}Mo_{0.71}O_{5.84}$ perovskite; and 5) the hysteresis loop of

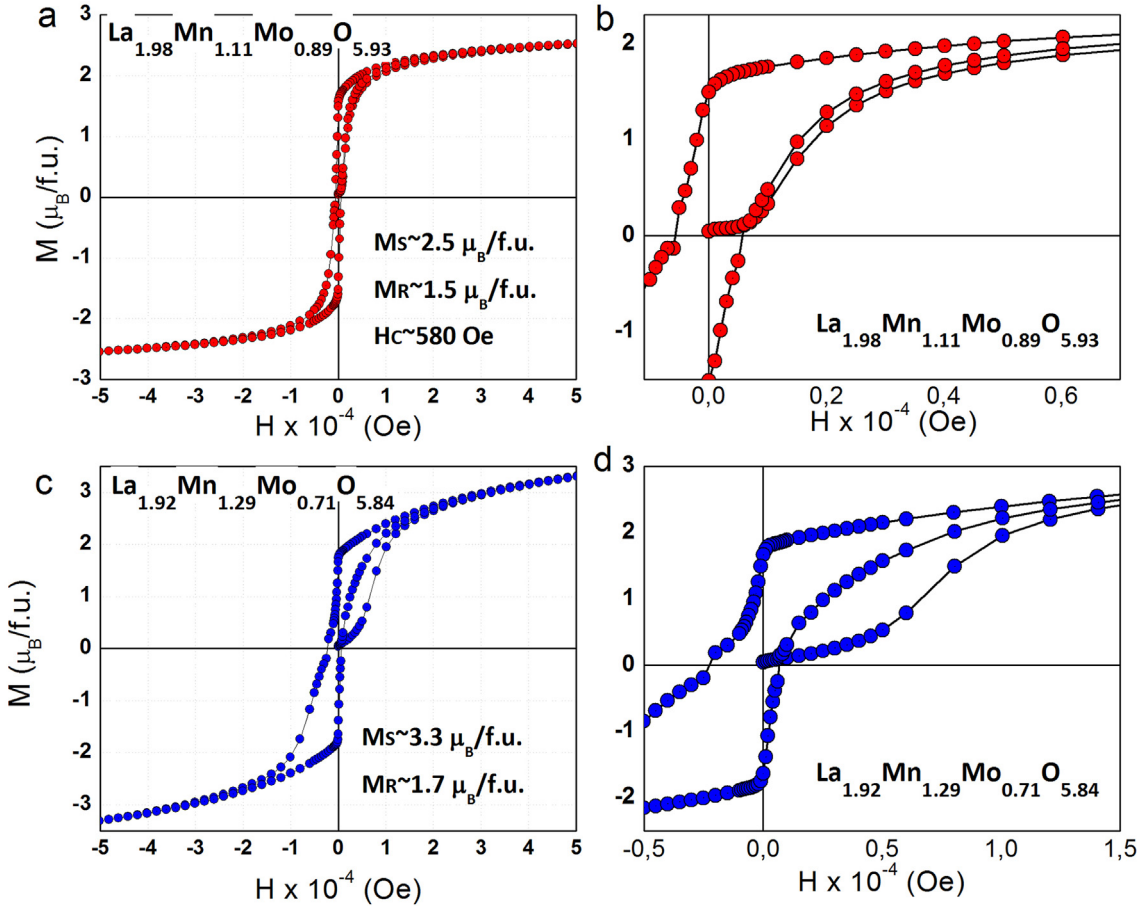

Fig. 7. Hysteresis loop of **a)** $La_{1.98}Mn_{1.11}Mo_{0.89}O_{5.93}$ and **c)** $La_{1.92}Mn_{1.29}Mo_{0.71}O_{5.84}$ double perovskites at 5 K, and **b, d)** details in the low fields region, respectively.

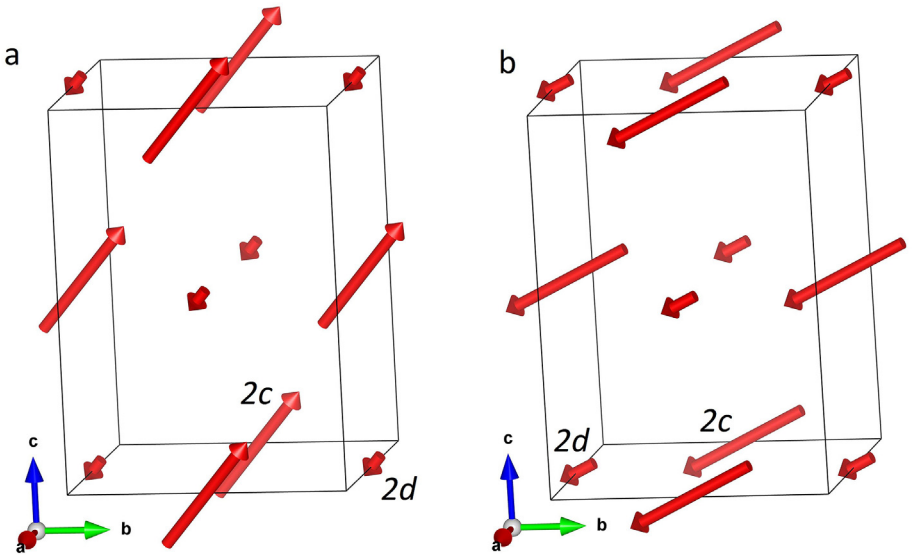

Fig. 8. Magnetic cell of **a)** $\mathbf{La_{1.98}Mn_{1.11}Mo_{0.89}O_{5.93}}$ and **b)** $\mathbf{La_{1.92}Mn_{1.29}Mo_{0.71}O_{5.84}}$, as refined from PND data at LT. Longer and shorter arrows represent the magnetic moments of $(Mn/Mo)_{2c}$ cations and $(Mn/Mo)_{2d}$ cations, respectively. The magnitude of arrows is illustrative and the represented magnetic moments are not comparable between cells.

$La_{1.92}Mn_{1.29}Mo_{0.71}O_{5.84}$ is different from the other one, a step-like behaviour at low fields and the virgin curve lying outside the loop are the key unusual features. Anyhow, the shape of the hysteresis loops suggests ferro or ferrimagnetic macroscopic behaviour for both compounds.

The magnetic cells obtained from refinements of LT PND data shed light on the issue. $La_{1.98}Mn_{1.11}Mo_{0.89}O_{5.93}$ is a ferrimagnetic perovskite because of the decompensated antiferromagnetic coupling of two ferromagnetic sub-lattices, with different magnetic moments associated to *2d* and *2c* octahedral sites. At 2 K the total net magnetic moment is high. Previous studies on Sr_2FeMoO_6 are in agreement with this result: the magnetic moments of Fe and Mo order ferrimagnetically [10,33]. $La_{1.92}Mn_{1.29}Mo_{0.71}O_{5.84}$ is a ferromagnetic perovskite that results from the ferromagnetic coupling of analogous ferromagnetic sub-lattices.

In these double perovskites, multiple magnetic interactions between $d^n - d^n$ metal transition cations are possible, arising from $(Mn/Mo)_{2c}$–O–$(Mn/Mo)_{2d}$ superexchange paths. According to the empirical Goodenough-Kanamori rules [37] for 180° cation-anion-cation magnetic interactions, an antiferromagnetic coupling can be expected when two $d^5 - d^5$ cations interact. When $d^5 - d^1$ as well as $d^5 - d^2$ interactions establish through the superexchange paths, a ferromagnetic coupling can take place. However, the situation changes when the (Mn/Mo)–O–(Mn/Mo) bond angles decrease below a critical value $\delta_C < 180°$. For an intermediate angular range $135° < \delta_C < 150°$, Goodenough claims that it is reasonable to expect a sign change for some interactions. Interestingly, the bond angles in both perovskites are around the upper limit of the critical range (~150°).

The $La_{1.98}Mn_{1.11}Mo_{0.89}O_{5.93}$ perovskite is highly ordered (see 2*c* and 2*d* occupancies in Table 1), since the disorder in the 2*c* site is only 1% while it is 12% in the 2*d* site. This situation is represented in Fig. 9a. The perovskite structure is viewed along the [001] direction, and to facilitate the analysis it is simplified representing only Mn and Mo cations as full and empty circles respectively, and La^{3+} and O^{2-} are omitted. Due to the disorder, 88% of all the possible paths correspond to Mn_{2c}–O–Mo_{2d} with mainly $d^5 - d^1$ interactions, but also some $d^5 - d^2$, both antiferromagnetic interactions considering that the average Mn_{2c}–O–Mo_{2d} angles are 149° (see Table 3). Likewise, 11% correspond to Mn_{2d}–O–Mn_{2c} paths (purple (in the web version) circle in Fig. 9a) where the $d^5 - d^5$ interactions could be ferromagnetic for the same average angles. Only 1% concern Mo_{2d}–O–Mo_{2c} paths. This situation is compatible with the refined magnetic cell, where the two ferromagnetic sub-lattices are antiferromagnetically aligned due to the majority of available antiferromagnetic Mn_{2c}–O–Mo_{2d} paths. Each ferromagnetic sub-lattice comes from the total behaviour explained according Goodenough-Kanamori rules, see arrows in Fig. 9a.

The same analysis of the possible superexchange paths in $La_{1.92}Mn_{1.29}Mo_{0.71}O_{5.84}$, represented in Fig. 9b, shows that 70% are Mn_{2c}–O–Mo_{2d} paths with an average bond angle of 150° (see Table 3), and hence antiferromagnetic interactions might occur. Only 30% are Mn_{2c}–O–Mn_{2d} paths, see Fig. 9b. Then both $d^5 - d^5$ and $d^5 - d^4$ ferromagnetic interactions for an average

Table 6
Stoichiometric coefficients for magnetic ions per site in both perovskites (*a*, *b*, *c* and *d*), and: per site theoretical (μ^{site}_{theo}) and refined ($\mu^{site}_{refined}$) magnetic moments, and Ferro (μ^{Ferro}_{theo}) and Ferri (μ^{Ferro}_{theo}) theoretical magnetic moments according to: $|\mu^{2c}_{theo} \pm \mu^{2d}_{theo}|$. Bold numbers were obtained from Rietveld refinements.

Site	*a*	*b*	*c*	*d*	μ^{site}_{theo} (μ_B/site)	$\mu^{site}_{refined}$ (μ_B/site)	μ^{Ferro}_{theo} (μ_B/f.u.)	μ^{Ferri}_{theo} (μ_B/f.u.)
$\mathbf{La_{1.98}Mn_{1.11}Mo_{0.89}O_{5.93}}$								
2*c*	0.988	0.0	0.010	0.002	4.962	**4.9**	6.79	3.14
2*d*	0.120	0.0	0.740	0.113	1.824	**1.0**		
$\mu^{refined}$ (μ_B/f.u.)							**3.90**	
$\mathbf{La_{1.92}Mn_{1.29}Mo_{0.71}O_{5.84}}$								
2*c*	0.9	0.1	0	0	4.90	**2.783**	7.42	2.38
2*d*	0.27	0.02	0.34	0.37	2.52	**0.807**		
$\mu^{refined}$ (μ_B/f.u.)							**3.59**	

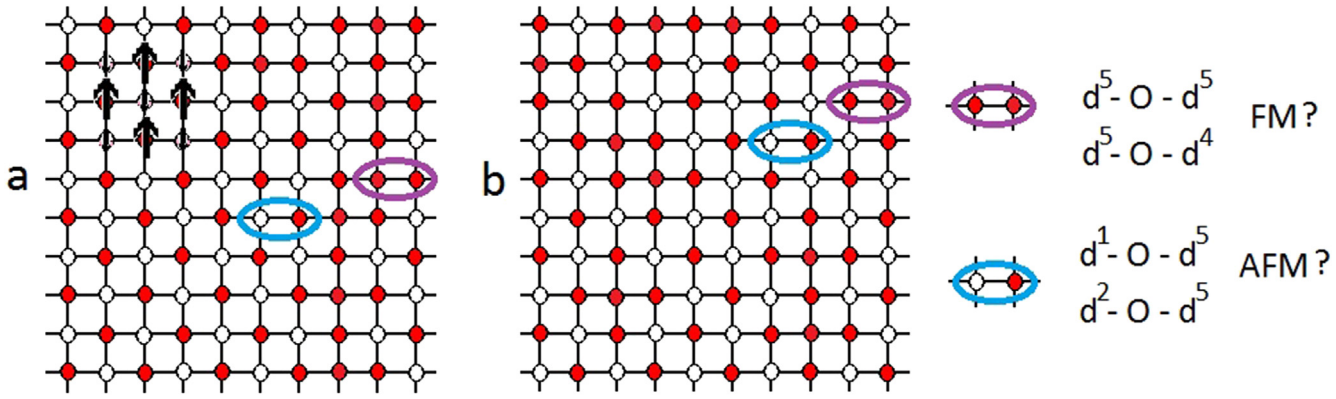

Fig. 9. View of 2D-statistical distribution of Mn (full circles) and Mo (empty circles) ions over the two octahedral sites in a) **$La_{1.98}Mn_{1.11}Mo_{0.89}O_{5.93}$** and b) **$La_{1.92}Mn_{1.29}Mo_{0.71}O_{5.84}$** monoclinic perovskites. Big arrows and little arrows represent the 2*c* and 2*d* ferromagnetic sub-lattices respectively.

Mn_{2c}–O–Mn_{2d} angle of 150° become available because of the presence of Mn^{2+} and Mn^{3+}, as confirmed by XES. In this scenario, again two antiferromagnetically coupled sub-lattices are expected for the whole behaviour. Then, if we consider only the localized magnetic interactions, the model seems inadequate to explain the long range magnetic behaviour.

The higher Mn ions content in octahedral *2c* site, when compared to the first perovskite, is not the only difference between both materials. The joint presence of Mn^{2+}/Mn^{3+} pairs may be enabling some ferromagnetic double-exchange interaction and thus increasing the magnetic ordering temperature in about 50 K. The presence of such Zener double exchange could add to the delocalized characteristics of both d^1 and d^2 unpaired electrons from Mo^{5+} and Mo^{4+} ions. Although the first perovskite have Mo^{4+} and Mo^{5+} ions too, the Mn^{2+}/Mn^{3+} double exchange of the $La_{1.92}Mn_{1.29}Mo_{0.71}O_{5.84}$ perovskite could change the long range magnetic behaviour from ferri to ferromagnetic.

5. Conclusions

Two new double perovskites, $La_{1.98}Mn_{1.11}Mo_{0.89}O_{5.93}$ and $La_{1.92}Mn_{1.29}Mo_{0.71}O_{5.84}$ were synthesized by the solid state method at 1400 °C for 12 h in Ar atmosphere, with minor impurities. Their compositions were determined by the joint Rietveld refinement of PXRD and PND data.

Their structures are monoclinic with space group $P2_1/n$ and β angles of approximately 90°. Similar lattices parameters *a*, *b* and *c* were obtained. The Mn and Mo occupancies of the octahedral *2d* and *2c* sites reveal that both compounds are highly ordered. Only 1% of disorder is found in *2c* sites and 12% in *2d* sites in the $La_{1.98}Mn_{1.11}Mo_{0.89}O_{5.93}$ structure. For $La_{1.92}Mn_{1.29}Mo_{0.71}O_{5.84}$, 30% of disorder is found in 2*d* sites whereas *2c* sites are completely ordered. Preferential occupancy of *2c* sites by Mn cations, and of *2d* sites by Mo cations is revealed. Distorted octahedra are found in the two perovskites, especially in *2c* sites of $La_{1.92}Mn_{1.29}Mo_{0.71}O_{5.84}$. The tilt system for the space group $P2_1/n$ is $a^-b^-c^+$. Our results confirm the significant tilting of the octahedra in these perovskites, with tilt angles around 15°.

The refinement results indicate that La^{3+} and O^{2-} vacancies are introduced in the monoclinic structure of both compounds during the synthesis. This is interesting for the potential application as SOFC's electrodes, separation membrane components, catalysts, etc.

The oxidation state for Mn and Mo ions was established by XES. Exclusively Mn^{2+} ($3d^5$) cations are found in $La_{1.98}Mn_{1.11}Mo_{0.89}O_{5.93}$. Mn^{2+} and Mn^{3+} ($3d^4$) coexist in the $La_{1.92}Mn_{1.29}Mo_{0.71}O_{5.84}$ structure. In both samples Mo^{4+} ($4d^1$) and Mo^{5+} ($4d^2$) cations are present.

The magnetic characteristics were analysed from susceptibility vs T and hysteresis loops. $La_{1.98}Mn_{1.11}Mo_{0.89}O_{5.93}$ shows a complex magnetic behaviour with average transition temperatures $T_C = 139$ K and $\theta_{Weiss} = 114$ K. At 126 K irreversibility between ZFC and FC curves can be observed. The experimental paramagnetic moment is in the range 3.05–3.09 μ_B. The magnetization thermal evolution of $La_{1.92}Mn_{1.29}Mo_{0.71}O_{5.84}$ corresponds to a typical ferromagnetic compound. The transition temperatures are 50 K lower with respect to the other perovskite. Similarly, the ZFC and FC curves diverge at a temperature 50 K below that corresponding to $La_{1.98}Mn_{1.11}Mo_{0.89}O_{5.93}$. Its paramagnetic moment is higher than for the other one: 3.84 μ_B.

The magnetic cells of both perovskites were determined by Rietveld refinement of PND at LT. $La_{1.98}Mn_{1.11}Mo_{0.89}O_{5.93}$ shows uncompensated ferrimagnetic behaviour as a result of the antiferromagnetic coupling of two ferromagnetic sub-lattices associated to *2d* and *2c* sites. Considering the structural disorder, the predominant superexchange interactions in each magnetic sublattice occur along $(Mn^{2+})_{2c}$–O–$(Mo^{5+}/Mo^{4+})_{2d}$ paths. For a bond angle around 150° the $3d^5$ and $4d^1/4d^2$ magnetic moments could align antiferromagnetically. Further study is required for a complete magnetic description of this $La_{1.98}Mn_{1.11}Mo_{0.89}O_{5.93}$ perovskite, thus enabling to analyze its applicability in magnetic devices.

On the other hand, $La_{1.92}Mn_{1.29}Mo_{0.71}O_{5.84}$ shows a ferromagnetic behaviour at LT, resultant from the ferromagnetic alignment of two ferromagnetic sublattices related to *2d* and *2c* sites. Coincidently, the $(Mn^{2+})_{2c}$–O–$(Mo^{5+}/Mo^{4+})_{2d}$ paths are the major pathways for superexchange interactions of antiferromagnetic nature in each path. Thus, global ferrimagnetism would be expected. However, the simultaneous presence of Mn^{2+}/Mn^{3+} pairs in this perovskite may be enabling some ferromagnetic Zener double-exchange interactions, thus increasing the magnetic ordering temperature in about 50 K. The consequently electronic delocalization could add to the Mo electrons itinerant behaviour, then modifying the overall magnetic response of $La_{1.92}Mn_{1.29}Mo_{0.71}O_{5.84}$.

To the best of our knowledge the dependence of the magnetic properties of these perovskites with the Mn and Mo ions in B and B′ sites is quite interesting and contributes to the understanding of the magnetic behaviour of double perovskites.

Acknowledgements

R.E.C. is member of CONICET and thanks support from Consejo Nacional de Investigaciones Científicas y Técnicas (CONICET), PIP #

11220120100360, the Agencia Nacional de Promoción Científica y Tecnológica (ANPCyT), PICT-2013-2149 and the Secretaría de Ciencia y Tecnología de la Universidad Nacional de Córdoba (SECyT-UNC), Res. #103/15. G. N. is member of CONICET and thanks the support of ANPCyT PICT07-819, CONICET PIP 11220090100448 and by SeCTyP-UNCuyo 06/C313. We gratefully acknowledge the Institut Laüe Langevin (ILL) (Grenoble, France) for access to D2B powder diffractometers.

Appendix A. Supplementary data

Supplementary data related to this article can be found at http://dx.doi.org/10.1016/j.jallcom.2016.04.169.

References

[1] K.-I. Kobayashi, T. Kimura, H. Sawada, K. Terakura, Y. Tokura, Nature 395 (1998) 677.
[2] D.G. Franco, V.C. Fuertes, M.C. Blanco, M.T. Fernández-Díaz, R.D. Sánchez, R.E. Carbonio, J. Solid State Chem. 194 (2012) 385.
[3] V.C. Fuertes, M.C. Blanco, D.G. Franco, J.M. De Paoli, R.D. Sánchez, R.E. Carbonio, Mater. Res. Bull. 46 (2011) 62.
[4] V.C. Fuertes, M.C. Blanco, D.G. Franco, J.M. De Paoli, E.V. Pannunzio Miner, R.D. Sánchez, M.T. Fernández-Díaz, R.E. Carbonio, Phys. B Condens. Matter 404 (2009) 2717.
[5] M.C. Blanco, J.M. De Paoli, S. Ceppi, G. Tirao, V.M. Nassif, J. Guimpel, R.E. Carbonio, J. Alloys Compd. 606 (2014) 139.
[6] D.G. Franco, R.E. Carbonio, E.E. Kaul, G. Nieva, J. Magn. Magn. Mater 346 (2013) 196.
[7] D.G. Franco, R.E. Carbonio, G. Nieva, J. Solid State Chem. 207 (2013) 69.
[8] R.M. Pinacca, M.C. Viola, J.A. Alonso, J.C. Pedregosa, R.E. Carbonio, J. Mater. Chem. 15 (2005) 4648.
[9] Z. Szotek, W.M. Temmerman, A. Svane, L. Petit, G.M. Stocks, H. Winter, J. Magn. Magn. Mater. 272–276 (2004) 1816–1817.
[10] O. Chmaissem, R. Kruk, B. Dabrowski, D. Brown, X. Xiong, S. Kolesnik, et al., Phys. Rev. B 62 (2000) 14197.
[11] T.K. Mandal, A.M. Abakumov, M.V. Lobanov, M. Croft, V.V. Poltavets, M. Greenblatt, Chem. Mater 20 (2008) 4653.
[12] Y.-H. Huang, Science 312 (2006) 254.
[13] Y.-H. Huang, R.I. Dass, J.C. Denyszyn, J.B. Goodenough, J. Electrochem. Soc. 153 (2006) A1266.
[14] P. Glatzel, U. Bergmann, Coord. Chem. Rev. 249 (2005) 65.
[15] H.M. Rietveld, J. Appl. Crystallogr. 2 (1969) 65.
[16] J. Rodríguez-Carvajal, Phys. B Condens. Matter 192 (1993) 55.
[17] G. Tirao, S. Ceppi, A.L. Cappelletti, E.V. Pannunzio Miner, J. Phys. Chem. Solids 71 (2010) 199.
[18] G. Vankó, T. Neisius, G. Molnár, F. Renz, S. Kárpáti, A. Shukla, F.M.F. de Groot, J. Phys. Chem. B 110 (2006) 11647.
[19] S. Ceppi, A. Mesquita, F. Pomiro, E.V. Pannunzio Miner, G. Tirao, J. Phys. Chem. Solids 75 (2014) 366.
[20] G. V. Bazuev, G. P. Shveikin, O. V. Makarova, Dokl. Akad. Наук. СССР (Reports Academic Sci. SSSR) 286(4) (1986) 890.
[21] G.V. Bazuev, O.V. Makarova, G.P. Shveikin, Russ. J. Inorg. Chem. 32 (1987) 2550.
[22] J. Lee, B. Kim, B.H. Kim, B.I. Min, S. Kolesnik, O. Chmaissem, J. Mais, B. Dabrowski, H.J. Shin, D.H. Kim, H.J. Lee, J.-S. Kang, Phys. Rev. B 80 (2009) 205112.
[23] A. Muñoz, J.A. Alonso, M.T. Casais, M.J. Martínez-Lope, M.T. Fernández-Díaz, J. Phys. Condens. Matter 14 (2002) 8817.
[24] R.D. Shannon, Acta Crystallogr. Sect. A 32 (1976) 751.
[25] V.F. Sears, Neutron News 3 (3) (1992) 26.
[26] A.M. Glazer, Acta Crystallogr. Sect. B Struct. Crystallogr. Cryst. Chem. 28 (1972) 3384.
[27] D.D. Sarma, Curr. Opin. Solid State Mater. Sci. 5 (2001) 261.
[28] J.A. Alonso, M.J. Martínez-Lope, M.T. Casais, T.M. Fernández-Díaz, Inorg. Chem. 39 (2000) 917.
[29] B.E. Day, N.D. Bley, H.R. Jones, R.M. McCullough, H.W. Eng, S.H. Porter, P.M. Woodward, P.W. Barnes, J. Solid State Chem. 185 (2012) 107.
[30] T. Nakamura, Y. Gohshi, Chem. Lett. 3 (1975) 1171.
[31] A.K. Azad, S.-G. Eriksson, S.A. Ivanov, R. Mathieu, P. Svedlindh, J. Eriksen, H. Rundlöf, J. Alloys Compd. 364 (2004) 77.
[32] G. Alejandro, D.G. Lamas, L.B. Steren, J.E. Gayone, G. Zampieri, A. Caneiro, M.T. Causa, M. Tovar, Phys. Rev. B 67 (2003) 064424.
[33] R. Ben Hassine, W. Cherif, J.A. Alonso, F. Mompean, M.T. Fernández-Díaz, F. Elhalouani, J. Alloys Compd. 649 (2015) 996.
[34] A. Poddar, C. Mazumdar, J. Alloys Compd. 502 (2010) 13.
[35] D. Sanchez, J.A. Alonso, M. García-Hernández, M.J. Martínez-Lope, J.L. Martínez, Phys. Rev. B 65 (2002) 104426.
[36] P.A. Joy, S.K. Date, J. Magn. Magn. Mater 210 (2000) 31.
[37] J.B. Goodenough, Magnetism and the Chemical Bond, John Wiley & Sons, Inc, Cambridge, Massachussets, 1963.